Article

Minimal Surfaces in Porous Materials: X-Ray Image-Based Measurement of the Contact Angle and Curvature in Gas Diffusion Layers to Design Optimal Performance of Fuel Cells

Mohammad Javad Shojaei,* Branko Bijeljic, Yihuai Zhang, and Martin J. Blunt

Read Online

ACCESS | 📊 Metrics & More | 📰 Article Recommendations

Water distribution inside gas diffusion layer with 20% PTFE coating
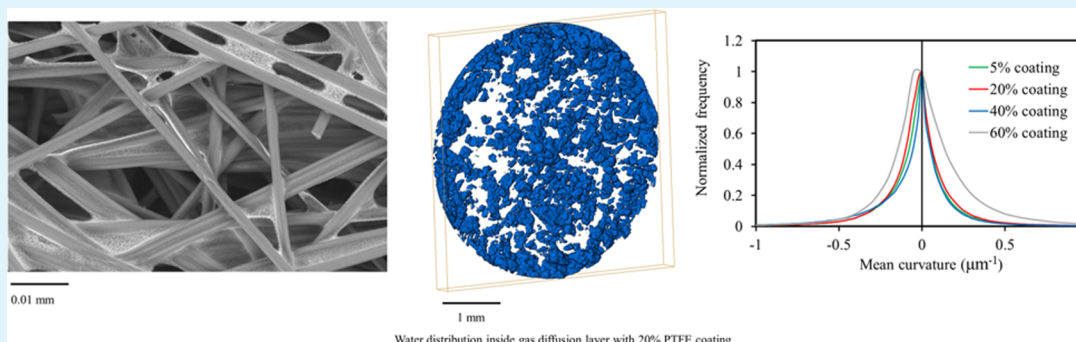
ABSTRACT: We inject water at a low flow rate through gas diffusion layers containing different percentages of polytetrafluoroethylene (PTFE) coating: 5, 20, 40, and 60%. We use high-resolution three-dimensional X-ray imaging to identify the arrangement of fibers, water, and air in the pore space. We also quantify the contact angle and meniscus curvature once the water has spanned the layer, flow has ceased, and water has reached a position of equilibrium. The average contact angle and water pressure at breakthrough increase with the amount of coating, although we see a wide range of contact angles with values both above and below 90°, indicating a mixed-wet state. We identify that the menisci form minimal surfaces (interfaces of zero curvature) consistent with pinned gas-water-solid contacts. Scanning electron microscopy images of the fibers show that the coated fibers have a rough surface. Between 93 and 100% of the contacts identified were found on the rough, hydrophobic, coated fibers or at the boundary between uncoated (hydrophilic) and coated (hydrophobic) regions; we hypothesize that these contacts are pinned. The one exception is the 60% PTFE layer, which shows distinctly hydrophobic properties and a negative capillary pressure (the water pressure is higher than that of air). The presence of minimal surfaces suggests that the water and gas pressures are equal, allowing water to flow readily without pressure build-up. From topological principles, the negative Gaussian curvature of the menisci implies that the fluid phases are well connected. The implication of these results is explored for the design of porous materials where the simultaneous flow of two phases occurs over a wide saturation range.

KEYWORDS: *gas diffusion layer, X-ray computed tomography, wettability, contact angle, minimal surfaces*

INTRODUCTION

Multiphase flow in porous media is ubiquitous in natural and engineered settings, from hydrogen and carbon dioxide storage deep underground, and water infiltration in soil, to water and gas transport in electrochemical devices, and droplet flow in surgical masks.[1] Optimal behavior is normally when one of two opposing goals is achieved: either multiphase flow results in the trapping of one fluid phase in the pore structure (for instance, for storage or to prevent water-borne infection through a surgical mask), or the reverse in which two or more fluid phases can flow as readily as possible over a wide saturation range (for oil recovery, and in electrochemical devices where gases and water need to be transported through porous membranes). In this study, we will focus on
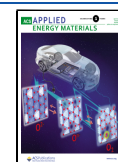
investigating and proposing the conditions ideal for the simultaneous flow of gas and water in gas diffusion layers, GDLs, to provide favorable performance in a fuel cell.

It is well known that to maximize trapping, and to repel a phase from a porous medium, one phase should be strongly wetting while the other, nonwetting phase, is preferentially

trapped in the larger regions of the pore space.[1] Less established are the conditions ideal for the simultaneous flow of two phases with little or no trapping. Work related to oil recovery in consolidated rock has suggested that flow is facilitated over a wide range of saturation for a mixed-wet state, where there is a range of contact angles between the two fluids and solid, with values both above and below 90°: the rock is not preferentially wetting to either phase.[2] Furthermore, the curvature of the menisci is close to zero: the interfaces form approximately minimal surfaces with equal and opposite principal curvatures. Topologically, the presence of minimal surfaces ensures well-connected phases.[3,4]

This paper will explore whether or not fluid menisci in fibrous materials can also form minimal surfaces, which then provides a guide to designing optimal flow conditions for the simultaneous flow of water and gas. In particular, we will study GDLs which are a component of polyelectrolyte membrane fuel cells. The membrane electrode assembly is the central part of fuel cells which includes the membrane, catalyst layers, and GDLs.[5-7] Hydrogen is pumped to the catalyst anode during fuel cell operation and oxidizes to form protons and electrons.[8,9] The product protons pass through the membrane and enter the catalyst cathode, while the negatively charged electrons go through a different path to generate electricity. Both electrons and protons meet at the cathode side and combine with oxygen to produce heat and water.[8,9] GDLs are responsible for gas and water transport and supporting external forces.[10-12] Produced water moves through the GDL in the opposite direction to the gaseous reactants and exits the fuel cell.[13] Water management is crucial in maximizing fuel cell efficiency as water accumulation plugs the GDL pores and decreases power generation.[14-16] Precoating GDLs with a hydrophobic agent such as polytetrafluoroethylene (PTFE) is common to form locally hydrophobic domains for better water transport and to prevent water accumulation:[17,18] the focus of this paper is to use a quantification of interfacial curvature and contact angle to explain why this is the case and how it can be used in the design of improved materials.

Several experimental studies have explored the effect of coating on GDL performance. Van Nguyen et al.[19] studied the change in capillary pressure related to the amount of hydrophobic coating. Vijay et al.[20] proposed a gradient in PTFE coating in GDLs for more effective water management. Lee and Huang[21] measured a 130° effective contact angle (measured through the water) on the outer surface of a coated GDL. They observed that an increase in hydrophobicity greatly improved the performance of the hydrogen pump. Chang et al.[22] showed that the maximum peak power density occurs at a 5% coating percentage (this is defined as the mass of the coating as a percentage of the original mass of the GDL). Lim and Wang[23] demonstrated that a 10% coating content produced higher power densities than 30% coatings. Experimental results by Park et al.[24] revealed that maximum fuel cell performance was achieved at a 20% PTFE content. Lin and Van Nguyen[25] reported that adding PTFE to GDLs improved gas and water transport, but excessive PTFE content caused water flooding in the catalyst layer. Similar findings by other researchers showed that either too high or too low PTFE content can be detrimental to fuel cell performance.[26,27]

To complement this experimental research, many numerical investigations have explored the effect of wettability on water management in GDLs. For instance, Qin et al.[28] suggested that water was removed more effectively at larger contact angles

around 150°. Zhou et al.[29] studied two-phase flow in GDLs using the finite element method and observed that a PTFE gradient design with a more hydrophobic GDL near the catalyst layer was preferred for better water management. A pore network modeling study by Sinha and Wang[30] showed that in a mixed-wet GDL water flows through a linked hydrophilic pore network, suppressing the finger-like liquid water structure in a hydrophobic GDL. Ira et al.[31] studied the role of wettability heterogeneity in GDLs using lattice Boltzmann simulation. They demonstrated that depending on their location, hydrophilic fibers might have positive or negative effects on water transport in the GDL.

These previous studies demonstrate that wettability is key to understanding the performance of GDLs. The contact angle through water on the exterior surface of a GDL has been measured using the pendant drop,[32] sessile drop,[33,34] and Wilhelmy plate methods.[35-37] However, the PTFE distribution inside the GDLs is heterogeneous, and their pore size and chemical composition are very different from the external surface.[38] For example, Mortazavi and Tajiri[39] demonstrated that adding PTFE on a raw GDL increases the contact angle significantly, but no change in the externally measured contact angle was observed for different weight percentages of PTFE. Moreover, the roughness and porosity of the surface significantly influence contact angle measurements.[40] In addition, the capillary pressure-water saturation relationship showed contact angle hysteresis for two-phase flow in GDLs.[41-43] Overall, it can be concluded that the external contact angle is not representative of the interior wettability of GDLs, which in turn controls multiphase flow.

The use of high-resolution X-ray imaging has transformed our understanding of multiphase flow in porous media.[44] The fibrous structure of GDLs and water flow have been imaged to study the gas-water capillary pressure and fluid distribution.[44-46] To quantify the contact angle from high-resolution three-dimensional images, AlRatrout et al.[47] developed an algorithm that calculates contact angles at the three-phase contact line of gas, water, and solids (the fibers). Recently, Liu et al.[48] employed this open-source code to calculate the distribution of the local contact angle inside different types of GDLs with 5% PTFE coating: they found a mean contact angle of 96−112° with a standard deviation of 24−37°. This work shows that GDLs have a range of contact angles in their interior with values both above and below 90°, indicating a mix of hydrophilic and hydrophobic surfaces.

In addition, the capillary pressure, the pressure difference between the gas and water, can be estimated from the curvature of the fluid menisci using the Young−Laplace equation:[49]

$$P_c = \sigma\kappa = \sigma(\kappa_1 + \kappa_2) = \sigma\left(\frac{1}{r_1} + \frac{1}{r_2}\right) \tag{1}$$

where σ is the interfacial tension between gas and water, r_1 and r_2 are the principal radii of curvature, and κ is the total curvature, which is the sum of the principal curvatures κ_1 and κ_2. This image-based measurement complements direct pressure recordings. Ideally, the capillary pressure should be as close to zero so that the water can escape the system with as low an excess pressure as possible. On the other hand, we do not wish the GDL to be water-wet (hydrophilic) as then the porous medium will retain water and a positive gas pressure will be required to remove it from the pore space.

A. Experimental apparatus

B. GDL preparation
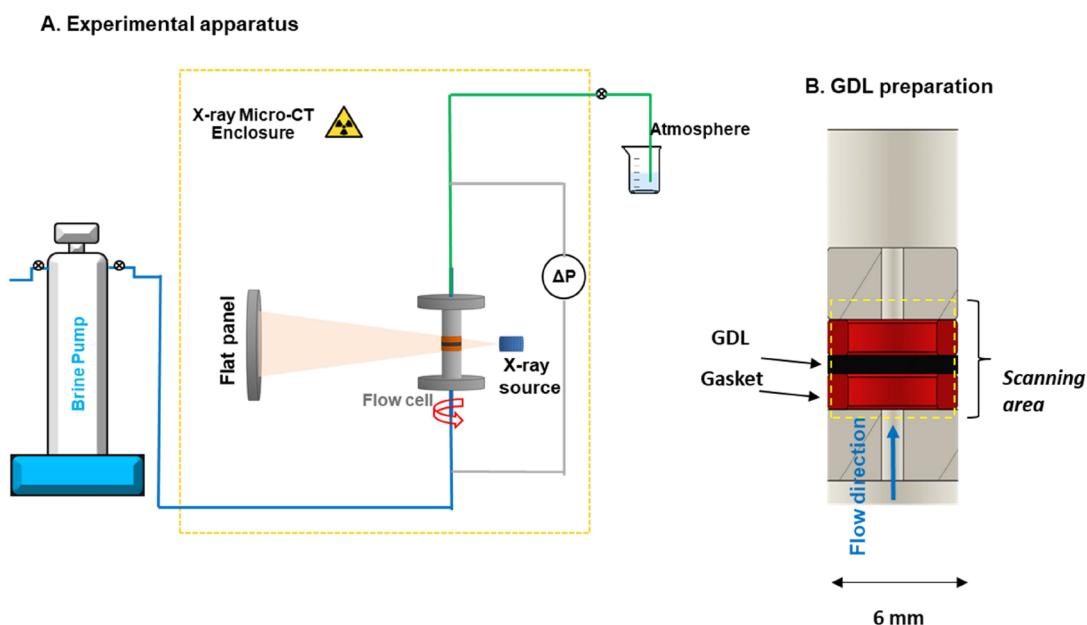
Figure 1. Schematic diagram of the experimental apparatus using a flow cell made of PEEK. (a) Experimental apparatus. (b) Details of the flow cell.

As discussed above, research to date has shown that ideal performance, meaning specifically optimal flow of gas and water through the GDL, is achieved when the originally hydrophilic fibers are partially coated with a hydrophobic material.[50] This results in a mixed-wet medium with both hydrophilic and hydrophobic surfaces, as shown by direct in situ contact angle measurements.[50] However, the best performance appears to be observed over a wide range of coating mass fractions, from 5 to 20%, with little apparent change in the externally measured contact angle.

In this study, we will inject water into GDLs with different coating percentages of 5, 20, 40, and 60%. The coating percentage is the percentage of the PTFE added mass compared to the original mass of the GDL. We will test the hypothesis that the favorable performance demonstrated by PTFE-coated GDLs is a consequence of the formation of minimal surfaces between gas and water. The presence of minimal surfaces will be demonstrated through measurements of the contact angle and curvature. We will show that the three-phase contacts of the two fluids with the fibers occur at the boundary between coated and uncoated regions, or on the rough coated fibers themselves: these contacts are pinned in place with hinging contact angles. This explains the range of local contact angle values observed. Minimization of surface energy at pinned contacts leads to minimal surfaces.[3] This has two desirable consequences. The first is that the pressure difference between water and gas is zero, which allows easy access of both fluids to the pore space. The second is that it guarantees good connectivity: from the Gauss–Bonnet theorem, the Gaussian curvature $G = \kappa_1\kappa_2 = 1/r_1r_2$ is related to the Euler characteristic of the phase surrounded by the meniscus (in this case water clusters) through:[4]

$$\int G \, dS = 4\pi\chi \tag{2}$$

The Euler characteristic, χ, measures the number of objects (water clusters) minus the number of holes in the clusters (trapped gas) minus the number of redundant loops (connections that can be cut without creating a new discrete

cluster of water). A large and negative Euler characteristic is indicative of a well-connected object.

The wider implication of this work is that we can use images and the analysis of the curvature and contact angle to determine conditions optimal for flow in porous materials. We suggest, in this specific instance, that minimal surfaces are observed for coating percentages in the range of 5–40%. Other criteria, including breakthrough capillary pressure for water, porosity, and mechanical strength, will determine the maximum operando performance within this range.

■ EXPERIMENTAL PROCEDURE

External Contact Angle Measurement. We imaged four GDLs of the same family (AvCarb MGL 370 Carbon Paper) with different amounts of coating: 5% (69% porosity measured from the dry image), 20% (67% porosity), 40% (66% porosity), and 60% (33% porosity). Advancing and receding contact angle measurements on the external surface of the GDLs were conducted on a sample at a 30° tilt with 1×1 cm^2 surface area at room temperature. The ImageJ Contact Angle Plugin was used for contact angle calculations. This plugin detects the edge of the droplet, fits an ellipse, and returns the contact angle values by drawing a tangent to the three-phase contact line. Moreover, we performed scanning electron microscopy (SEM) experiments to examine carbon fibers in more detail to distinguish coated and uncoated regions.

X-Ray Imaging. Figure 1 shows the experimental apparatus. The experiments were conducted in a flow cell made of polyether ether ketone (PEEK) that is X-ray-transparent. The GDL, a disk, with 6 mm diameter and 0.370 mm thickness, was clamped between two gaskets to avoid any leakage during the experiments. The imaging parameters of the Heliscan micro-CT scanner were set as follows using a flat panel detector: the photon source energy was 26 keV, the number of collected projections per sample was 2880, and the exposure time was 900 ms. The images had a voxel size of 2.05 μm.

We injected a brine solution made from deionized water with 15 weight% potassium iodide (KI). The interfacial tension between air and brine is 73.5 mN·m^{-1}.[51] The addition of KI was to aid the image contrast between solid (carbon fiber and PTFE), air, and water. This allowed for accurate segmentation by providing discrete X-ray attenuations for each phase. We assume that the addition of this salt does not affect the wettability of the GDL in the presence of air.
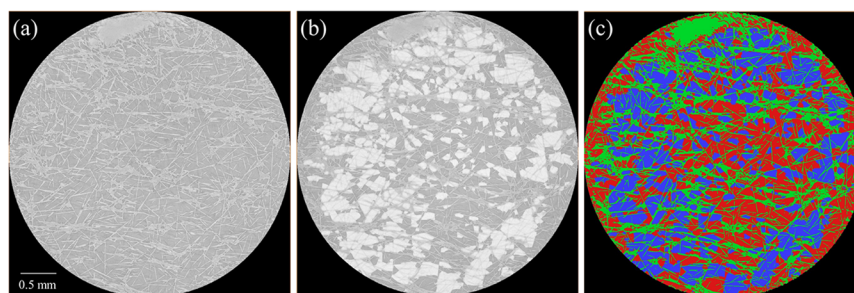
Figure 2. Gray-scale two-dimensional cross-sections of three-dimensional images of dry (a) and wet (b) scans and the corresponding segmented image (c) of GDLs with 5% PTFE. The wet scan was registered to the dry scan to have the same orientation. In (a), the fibers are the brighter phase. In (b), the doped brine is bright, the fibers are light gray, and the pore space is the darker gray. In (c), the fibers, air, and water are green, red, and blue, respectively.

High-precision low-flow rate Teledyne ISCO pumps were used to inject water vertically upward through the GDL at 7 μL/h, which continued for 30 mins after the breakthrough point (indicated by a sudden pressure drop). During the experiments, a high-precision pressure transducer, Keller PD-33, recorded the pressure difference between the inlet of the flow cell and the outlet which was connected to the atmosphere. One dry scan was taken before water injection and another 2 h after stopping the pump as depicted in Figure 2. There is no flow when the scans are taken, representing steady-state conditions. Because of the high quality of the scanned image, segmentation was performed with no initial filtering.

Image Processing, Segmentation, Contact Angle, and Curvature. After reconstruction, each image was registered to the dry scan image to have the same orientation using the image registration and resampling modules in commercial image analysis software, Avizo. Each image was segmented into three phases: fiber, water, and air. The interactive thresholding and watershed segmentation methods were used for dry scan and wet scan segmentation, respectively. These two methods were combined, as it was difficult to differentiate between the water and fibers in the wet scan. The quality of the segmentation was assessed by reference to the raw images, see Figure 2. Analysis was only performed on the part of the image containing the GDL to eliminate edge effects.

The distribution of the contact angle was found on each voxel at the three-phase contact line using the automatic method of AlRatrout et al.[47] The interface between air and water was extracted, and an unconstrained smoothing algorithm with a smoothing extent equal to 5 voxels was applied to this surface. We computed both principal curvature values, total curvature and Gaussian curvature on the smoothed surface.

■ RESULTS

Figure 3 shows three-dimensional images of the water for the four experiments. The water is well connected across the GDL, but the water clusters have a complex structure, forming branches and loops throughout the pore space.

Pressure Measurements. Figure 4 shows the pressure recorded in the experiments. This is equivalent to the pressure difference between the water and the ambient air before breakthrough. There is an approximately linear rise in pressure with time as the water progresses through the GDL. Once the water breaks through, that is spanning the GDL from the inlet to outlet, the pressure drops rapidly and falls to zero to within the sensitivity of the transducer. The time to breakthrough and the maximum pressure reached increase with the degree of PTFE coating in agreement with the findings of other researchers.[25,27,52] The maximum pressures recorded agree with the range observed in the literature of 3−6 kPa.[46,53] Once water is connected across the GDL, there is a negligible pressure difference because of flow across the sample: when
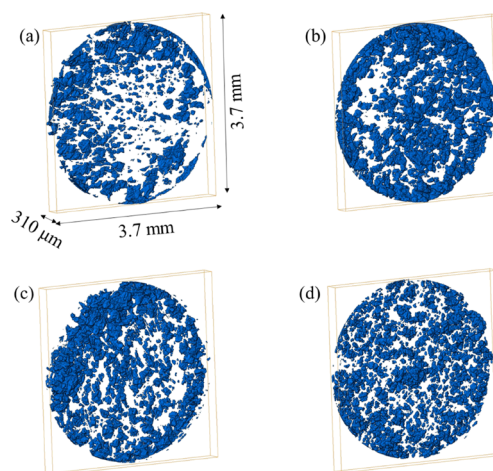

Figure 3. (a−d) show three-dimensional images of water (blue) in GDLs with 5, 20, 40, and 60% PTFE coating, respectively. The air and fibers are not shown.
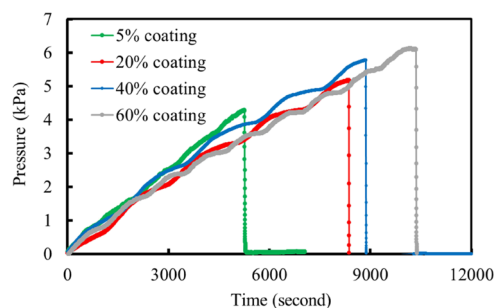
Figure 4. Measured pressure across the flow cell during water injection. This is equivalent to the pressure difference between water and the ambient air before breakthrough. The pressure rises until water breaks through—spans the GDL—and then drops to become zero to within the sensitivity of the transducer: at this point, the pressure records the undetectable pressure difference across the GDL in the water.

water reaches the outlet, the transducer only measures the pressure drop in the water itself, and not the pressure difference between air and water.
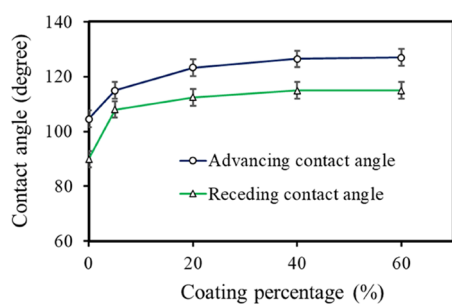
Contact Angle Measurements. Figure 5 shows the distribution of the contact angle for the different degrees of PTFE coating as well as the mode values—the peak of the distribution. There is a wide range of contact angles in all cases with values both above and below 90°. The mode value
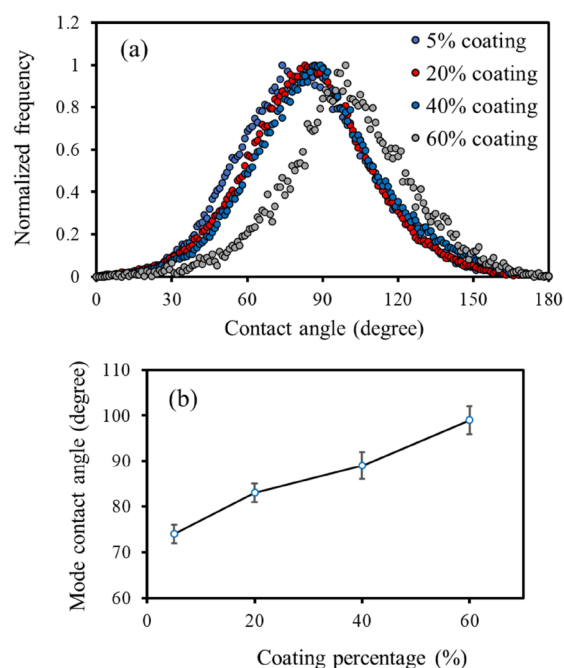
Figure 5. (a) Contact angle distributions computed on GDLs with different coating percentages. (b) Mode contact angle obtained from the data in (a). The error bar shows the standard deviation of the distribution.

increases with the degree of coating with noticeably higher values—indicating more strongly hydrophobic conditions—for 60% coating. The mode values and standard deviations of the distributions are in the range observed for different types of GDLs by Liu et al.;[48] however they studied systems with only a 5% coating and found average contact angles above 90°, whereas for 5% coating we find an average that is around 74°.

Consistent with previous work,[48] we find that the contact angles measured inside the GDL are, in most cases, lower (more hydrophilic) than those determined for a droplet on the external surface, as shown in Figure 6. Here for a coating

Figure 6. Advanced and receding contact angle measured on the outer surface of GDLs with different PTFE contents. The error bar shows the standard deviation of three measurements.

percentage of more than 20%, the external contact angle values are high and appear insensitive to the degree of coating—essentially, we are simply measuring the contact angle on PTFE alone.[54] However, within the pore space we have a mix of hydrophilic and hydrophobic regions where three-phase contacts are pinned at the boundary between the two types of material, as we show later.
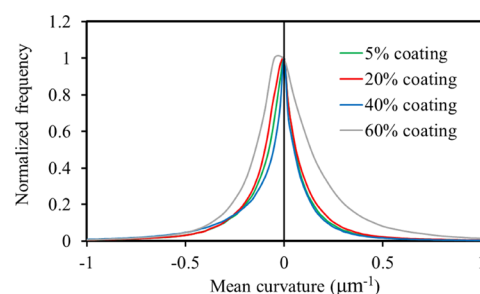
Figure 7. Distribution of total mean curvature κ for the menisci within the GDLs with different PTFE contents as presented in the legend. The bin size of the histogram is 0.006 μm^{-1}.

**Table 1. Average Total Curvatures and Capillary Pressure Using Eq 1 for Different GDLs[a]**

coating percentage (%)	mode curvature, κ (1/μm)	P_c (kPa)
5	0.00 ± 0.01	0.0 ± 0.8
20	0.000 ± 0.009	0.0 ± 0.7
40	0.000 ± 0.008	0.0 ± 0.6
60	−0.05 ± 0.01	−4 ± 1

[a]The uncertainty range calculated based on the values results using different segmentation methods.

Curvature and Capillary Pressure. Figure 7 shows the estimated distributions of curvature for the cases studied. In equilibrium, with no flow, the menisci arrange in the pore space with an almost zero total curvature, corresponding to a zero capillary pressure, eq 1. Table 1 shows the mode of the measured total curvature values: to within the uncertainty in the measurements, the curvature is zero for the 5, 20, and 40% coatings. We use the mode values to find a representative curvature, rather than the arithmetic mean, which is affected by large outlier values near the three-phase contacts where uncertainty in segmentation can affect the results significantly. Also note that the capillary pressure at rest is lower than that measured during water injection, Figure 4. Zero curvature interfaces are called minimal surfaces and are seen when surface energy is minimized while the contact lines are pinned.[3] As we show later, this is indeed the case in these experiments, where the contact lines lie at the borders between hydrophilic and hydrophobic regions of the fibers. The only exception is the case with 60% coating. As evident from the contact angle, Figure 5, the degree of coating is such that the medium is almost entirely hydrophobic. In this case, the contact lines have to lie on coated fibers (see later for a confirmation of this interpretation); the contact angles are larger than 90°, and the fluid menisci have a distinctly negative curvature and capillary pressure—the water pressure is higher than the pressure in the air.

Gaussian Curvature and Connectivity. Figure 8 shows the distributions of curvature decomposed into histograms where both principal curvatures are positive (this would represent menisci in clearly hydrophilic regions of the pore space), both curvatures are negative (in hydrophobic regions) and where the two curvatures are of opposite sign (representing pinned contacts and mixed-wet conditions). We see that virtually all the interfaces have a negative Gaussian curvature: while the mean curvature is close to zero, this does not mean that the menisci are flat; instead in one direction water bulges into air, while in the other direction air bulges into water.
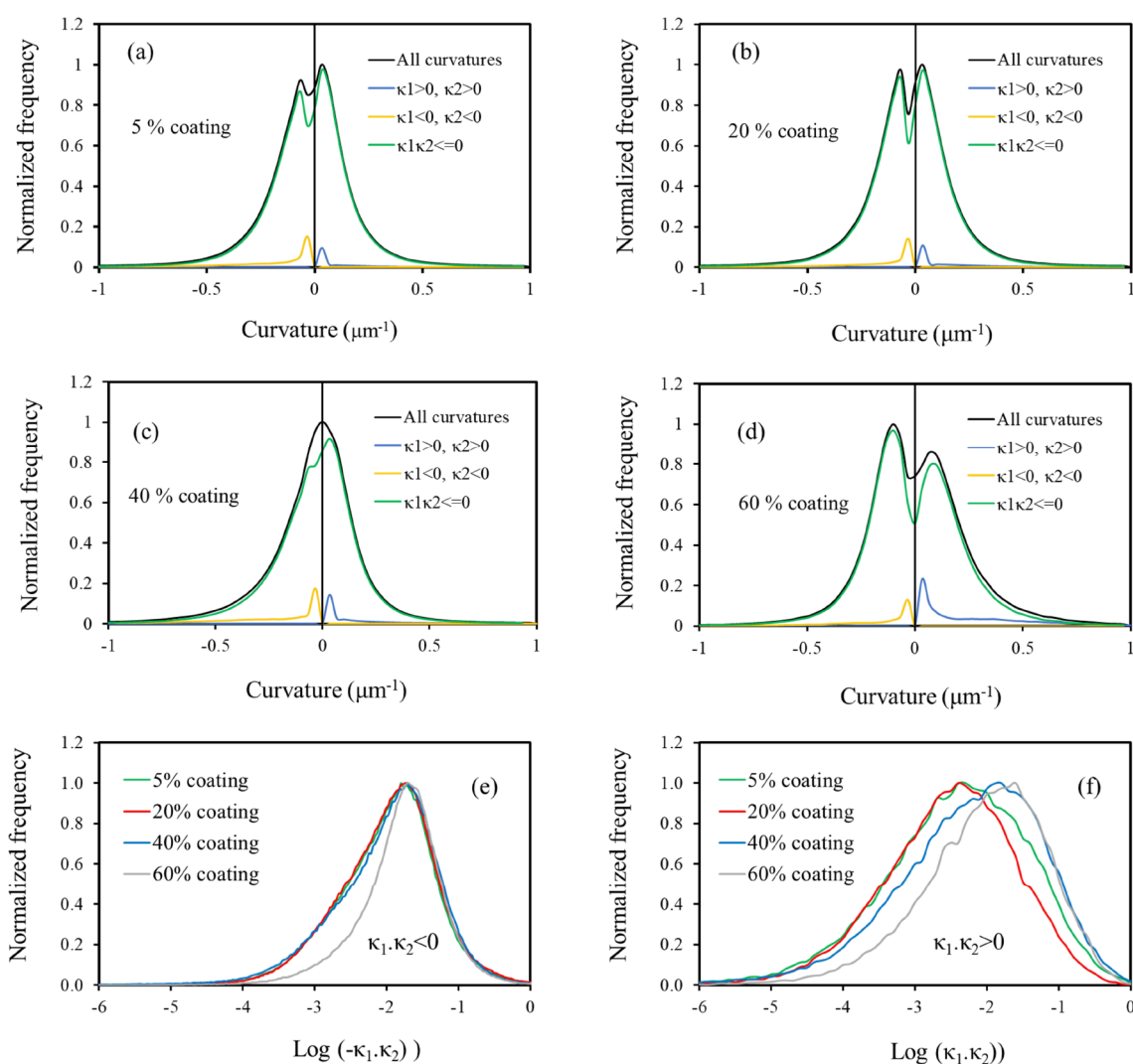
Figure 8. (a–d) Distributions showing different curvature values for $\kappa_1 > 0$, $\kappa_2 > 0$ (blue), $\kappa_1 < 0$, $\kappa_2 < 0$ (yellow), and $\kappa_1.\kappa_2 < 0$ (green) for GDLs with different PTFE contents as presented in the legends. (e) Gaussian curvature distribution for the different GDLs where the Gaussian curvature is negative. The x-axis is logarithmic, showing the base 10 logarithm of $-\kappa_1\kappa_2$ measured in units of μm^{-2}. (f) Same as (e) but where the Gaussian curvature is positive.

Note that the magnitude of the Gaussian curvature is not zero, but of order $0.01-0.1 \ \mu m^{-2}$: the two principal curvatures have—to within measurement uncertainty—equal size but opposite signs. The same phenomenon has been seen in oil–water menisci in porous rocks[2]— the difference is that in the GDLs an even greater fraction of the interface has a negative Gaussian curvature, representing conditions closer to true minimal surfaces than encountered in the more restricted, lower porosity, pore space of consolidated rock under flowing conditions.

Using eq 2, the connectivity defined through the Euler characteristic can be quantified from integrating the Gaussian curvature of the menisci. In this calculation, we ignore the contribution of the solid and contact lines, which add additional deficit curvature to the calculation.[50] Table 2 shows the normalized Euler characteristic (Euler characteristic per unit volume). The large negative values indicate that the water is well connected through the pore space, facilitating its flow.

Pinned Contacts. It was challenging to distinguish coated and uncoated fibers from X-ray images; the difference in

Table 2. Normalized Euler Characteristic (Euler Characteristic per Unit Volume) Computed Using the Integral of the Gaussian Curvature over the Fluid Menisci, Eq 2[a]

coating percentage (%)	normalized Euler characteristic (mm^{-3})
5	−9903
20	−13,571
40	−9000
60	−6790

[a]The large negative numbers indicative of well-connected phases.

contrast is insufficient to allow an automatic segmentation of the two types of fibers. To understand the structure of the GDL in more detail, we performed SEM experiments at different resolutions. Figure 9 shows that the coated fibers have a rough surface, in contrast to the smooth, hydrophilic uncoated regions. Furthermore, the so-called coating percentage does not quantify the fraction of the surface that is hydrophobic: at 60%, almost all the surfaces are coated with PTFE.
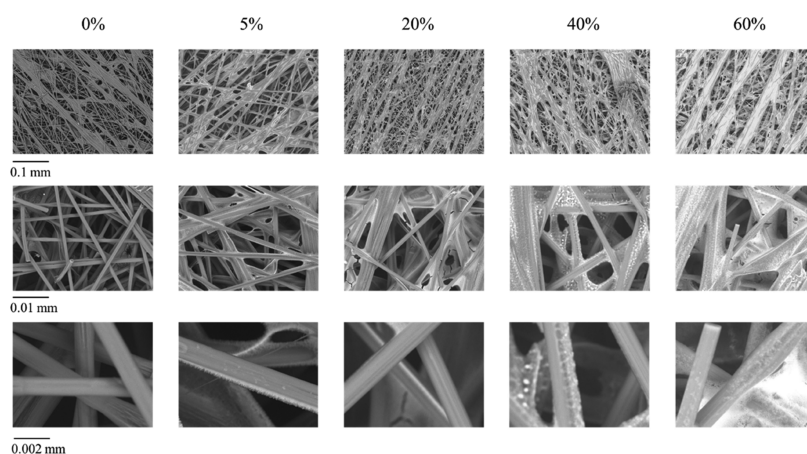
Figure 9. First, second, and third rows are SEM images of GDLs at different resolutions for the coating percentage depicted in the legend. The coated fibers, shown at highest resolution for the 40 and 60% cases, have rough surfaces, while the uncoated fibers (see the highest resolution 0, 5, and 20% images) are smooth.
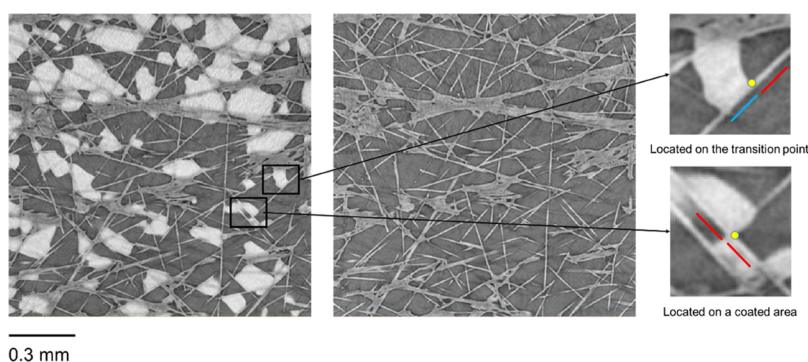
Figure 10. Illustration of how contacts were identified. A cross section of the 5% GDL. Using the wet (left) image, we first identified the three-phase contact between air, water, and solid, shown as the yellow dot in the magnified figure (right). Then from the dry scan (center) and the SEM images (Figure 9), we determine if the contact point is located on an uncoated fiber (blue), one that is coated (red), or at the boundary between two regions.

Using the SEM images as a guide, together with the registered wet and dry images, we manually identified contacts between water, air, and the fibers and categorized if these contacts lay on uncoated (hydrophilic) fibers, on the coated (hydrophobic) fibers or at the boundary, or transition region between them. This process is illustrated in Figure 10. To perform a quantitative analysis, for each GDL we selected a region 647 voxels across and identified the nature of each contact. The results are shown in Table 3.

The results show that more than 93% of the three-phase contacts lie at the boundary between parts of the fibers that are coated and uncoated—where there is a transition from hydrophilic to hydrophobic conditions—or on the rough, coated surfaces (Table 3). Contact lines can be pinned both on

rough surfaces and when there is a change in wettability.[1] We hypothesize that in our experiments these contacts are indeed pinned, in that the contact angle can vary without movement of the contact line: this explains why, in equilibrium, the menisci form minimal surfaces, maintaining good connectivity of the fluid phases and minimizing the pressure difference between them. The 60% coating though is an exception because almost all the surfaces are hydrophobic and all the contact points are found on the coated fibers, see Figure 9 and Table 3.

■ DISCUSSION AND CONCLUSIONS

GDLs in fuel cells need to allow the simultaneous flow of gases and water. Empirically this is achieved by coating the naturally hydrophilic carbon fibers with a hydrophobic coating, usually PTFE. We have used high-resolution X-ray imaging to observe the configuration of water within GDLs with different degrees of PTFE coating and to quantify the curvature and contact angle. We used the results to explain why this particular arrangement of wettability is favorable and to suggest how to design porous materials that allow the simultaneous flow of two phases over a wide saturation range.

We observe that the fluid menisci form minimal surfaces. These surfaces occur in equilibrium at pinned contact lines at the boundary between hydrophilic and hydrophobic parts of the fibers, or on the rough surfaces of the coated fibers.

Table 3. Identification of Contacts between Water, Air, and Solids for the GDLs Studied

coating percentage (%)	contacts on the uncoated area (hydrophilic)	contacts on the rough coated fibers (hydrophobic)	contacts at the boundary between hydrophobic and hydrophilic regions	total contact points
5	7	51	44	102
20	4	41	40	85
40	3	46	30	79
60	0	44	0	44

Minimal surfaces have two desirable features for multiphase flow. First, the pressure difference between the water and gas is zero, which means that no additional water pressure is required, preventing retention and clogging of the pore space. Second, from topological principles, minimal surfaces ensure well-connected phases: the water clusters contain many redundant loops which helps maintain the continuity of flow under operando conditions.

In our work, we found minimal surfaces for GDLs with 5, 20, and 40% coating with PTFE. The layer with a 60% coating had a markedly lower porosity and was more characteristically hydrophobic with higher average contact angles and a negative capillary pressure—that is the water pressure was higher than the surrounding air.

These experiments were not performed under flowing or indeed operando conditions. Hence, we cannot assess the role of other factors, such as fluid flow, compressibility, and electrical performance, in the overall efficiency of the GDL within a working fuel cell. However, this work does offer a simple way to determine if the porous medium characteristics are favorable for multiphase flow. This study provides a workflow for the characterization of wettability in GDLs which could be applied to the images acquired under flowing, operando conditions.

This work also has implications for other porous materials where multiphase flow is desirable. For instance, electrolyzers also need to allow the efficient transport of gases and water. It has been suggested that in electrolyzers and fuel cells multiphase flow is best achieved through having separate hydrophilic and hydrophobic channels or a structured porous design;[55−58] our work suggests an elegant alternative with fibers of different wettability to facilitate the formation of minimal surfaces.

■ AUTHOR INFORMATION

Corresponding Author

Mohammad Javad Shojaei − *Department of Earth Science and Engineering, Imperial College London, London SW7 2BX, U.K.;* ⓘ orcid.org/0000-0003-4927-921X; Email: m.shojaei@imperial.ac.uk

Authors

Branko Bijeljic − *Department of Earth Science and Engineering, Imperial College London, London SW7 2BX, U.K.*

Yihuai Zhang − *Department of Earth Science and Engineering, Imperial College London, London SW7 2BX, U.K.;* ⓘ orcid.org/0000-0001-5471-3450

Martin J. Blunt − *Department of Earth Science and Engineering, Imperial College London, London SW7 2BX, U.K.*

Complete contact information is available at:
https://pubs.acs.org/10.1021/acsaem.2c00023

Notes

The authors declare no competing financial interest.

■ REFERENCES

(1) Blunt, M. J. *Multiphase flow in permeable media: A pore-scale perspective*; Cambridge University Press, 2017.

(2) Lin, Q.; Bijeljic, B.; Berg, S.; Pini, R.; Blunt, M. J.; Krevor, S. Minimal surfaces in porous media: Pore-scale imaging of multiphase flow in an altered-wettability Bentheimer sandstone. *Phys. Rev. E* **2019**, *99*, No. 063105.

(3) Pérez, J. A new golden age of minimal surfaces. *Notices AMS* **2017**, *64*, 347−358.

(4) Allendoerfer, C. B.; Weil, A. The gauss-bonnet theorem for riemannian polyhedra. *Trans. Am. Math. Soc.* **1943**, *53*, 101−129.

(5) Barbir, F. PEM fuel cells. In *Fuel Cell Technology*; Springer, 2006, pp. 27−51.

(6) Wilde, P.; Mändle, M.; Murata, M.; Berg, N. Structural and physical properties of GDL and GDL/BPP combinations and their influence on PEMFC performance. *Fuel Cells* **2004**, *4*, 180−184.

(7) Kim, J. R.; Premier, G. C.; Hawkes, F. R.; Dinsdale, R. M.; Guwy, A. J. Development of a tubular microbial fuel cell (MFC) employing a membrane electrode assembly cathode. *J. Power Sources* **2009**, *187*, 393−399.

(8) Dutta, S.; Shimpalee, S.; Van Zee, J. Numerical prediction of mass-exchange between cathode and anode channels in a PEM fuel cell. *Int. J. Heat Mass Transfer* **2001**, *44*, 2029−2042.

(9) Mekhilef, S.; Saidur, R.; Safari, A. Comparative study of different fuel cell technologies. *Renew. Sustainable Energy Rev.* **2012**, *16*, 981−989.

(10) Ozden, A.; Shahgaldi, S.; Li, X.; Hamdullahpur, F. A review of gas diffusion layers for proton exchange membrane fuel cells—With a focus on characteristics, characterization techniques, materials and designs. *Prog. Energy Combust. Sci.* **2019**, *74*, 50−102.

(11) Ozden, A.; Alaefour, I. E.; Shahgaldi, S.; Li, X.; Colpan, C. O.; Hamdullahpur, F. Gas diffusion layers for PEM fuel cells: ex-and in-situ characterization. *Exerge. Energe. Environ. Dimension* **2018**, 695−727.

(12) Majlan, E.; Rohendi, D.; Daud, W.; Husaini, T.; Haque, M. Electrode for proton exchange membrane fuel cells: A review. *Renew. Sustainable Energy Rev.* **2018**, *89*, 117−134.

(13) Park, J.; Li, X. An experimental and numerical investigation on the cross flow through gas diffusion layer in a PEM fuel cell with a serpentine flow channel. *J. Power Sources* **2007**, *163*, 853−863.

(14) Okonkwo, P. C.; Otor, C. A review of gas diffusion layer properties and water management in proton exchange membrane fuel cell system. *Int. J. Energy Res.* **2021**, *45*, 3780−3800.

(15) Kim, S.-G.; Lee, S.-J. A review on experimental evaluation of water management in a polymer electrolyte fuel cell using X-ray imaging technique. *J. Power Sources* **2013**, *230*, 101−108.

(16) Lee, S. J.; Lim, N.-Y.; Kim, S.; Park, G.-G.; Kim, C.-S. X-ray imaging of water distribution in a polymer electrolyte fuel cell. *J. Power Sources* **2008**, *185*, 867−870.

(17) Lee, M.; Huang, X. An improved hydrophobic coating for the porous gas diffusion layer in a PEM-based electrochemical hydrogen pump to mitigate anode flooding. *Electrochem. Commun.* **2020**, *117*, No. 106777.

(18) Arif, M.; Cheung, S. C.; Andrews, J. Influence of Hydrophobicity and Porosity of the Gas Diffusion Layer on Mass Transport Losses in PEM Fuel Cells: A Simulation Study Supported by Experiments. *Energy Fuels* **2020**, *34*, 13010−13022.

(19) Van Nguyen, T.; Ahosseini, A.; Wang, X.; Yarlagadda, V.; Kwong, A.; Weber, A. Z.; Deevanhxay, P.; Tsushima, S.; Hirai, S. Hydrophobic gas-diffusion media for polymer-electrolyte fuel cells by direct fluorination. *J. Electrochem. Soc.* **2015**, *162*, F1451.

(20) Vijay, R.; Seshadri, S.; Haridoss, P. Gas diffusion layer with PTFE gradients for effective water management in PEM fuel cells. *Trans. Indian Inst. Met.* **2011**, *64*, 175−179.

(21) Lee, M.; Huang, X. Development of a hydrophobic coating for the porous gas diffusion layer in a PEM-based electrochemical hydrogen pump to mitigate anode flooding. *Electrochem. Commun.* **2019**, *100*, 39−42.

(22) Chang, H.-M.; Lin, C.-W.; Chang, M.-H.; Shiu, H.-R.; Chang, W.-C.; Tsau, F.-H. Optimization of polytetrafluoroethylene content in cathode gas diffusion layer by the evaluation of compression effect on the performance of a proton exchange membrane fuel cell. *J. Power Sources* **2011**, *196*, 3773−3780.

(23) Lim, C.; Wang, C. Effects of hydrophobic polymer content in GDL on power performance of a PEM fuel cell. *Electrochim. Acta* **2004**, *49*, 4149−4156.

(24) Park, S.; Lee, J.-W.; Popov, B. N. Effect of PTFE content in microporous layer on water management in PEM fuel cells. *J. Power Sources* **2008**, *177*, 457−463.

(25) Lin, G.; Van Nguyen, T. Effect of thickness and hydrophobic polymer content of the gas diffusion layer on electrode flooding level in a PEMFC. *J. Electrochem. Soc.* **2005**, *152*, A1942.

(26) Yan, W.-M.; Hsueh, C.-Y.; Soong, C.-Y.; Chen, F.; Cheng, C.-H.; Mei, S.-C. Effects of fabrication processes and material parameters of GDL on cell performance of PEM fuel cell. *Int. J. Hydrogen Energy* **2007**, *32*, 4452−4458.

(27) Lobato, J.; Cañizares, P.; Rodrigo, M.; Ruiz-López, C.; Linares, J. Influence of the Teflon loading in the gas diffusion layer of PBI-based PEM fuel cells. *J. Appl. Electrochem.* **2008**, *38*, 793−802.

(28) Qin, Y.; Li, X.; Du, Q.; Yin, Y.; Jiao, K. Effect of wettability on water removal from the gas diffusion layer surface in a novel proton exchange membrane fuel cell flow channel. *Int. J. Hydrogen Energy* **2013**, *38*, 12879−12885.

(29) Zhou, X.; Wu, L.; Niu, Z.; Bao, Z.; Sun, X.; Liu, Z.; Li, Y.; Jiao, K.; Liu, Z.; Du, Q. Effects of surface wettability on two-phase flow in the compressed gas diffusion layer microstructures. *Int. J. Heat Mass Transfer* **2020**, *151*, No. 119370.

(30) Sinha, P. K.; Wang, C.-Y. Liquid water transport in a mixed-wet gas diffusion layer of a polymer electrolyte fuel cell. *Chem. Eng. Sci.* **2008**, *63*, 1081−1091.

(31) Ira, Y.; Bakhshan, Y.; Khorshidimalahmadi, J. Effect of wettability heterogeneity and compression on liquid water transport in gas diffusion layer coated with microporous layer of PEMFC. *Int. J. Hydrogen Energy* **2021**, *46*, 17397−17413.

(32) Cheah, M. J.; Kevrekidis, I. G.; Benziger, J. B. Water slug formation and motion in gas flow channels: the effects of geometry, surface wettability, and gravity. *Langmuir* **2013**, *29*, 9918−9934.

(33) Lin, Y. C.; Chang, H. H.; Tsai, D. C.; Huang, R. H.; Shieu, F. S. Reduced graphene oxide−coated anode gas diffusion layer for performance enhancement of proton-exchange membrane fuel cell. *Int. J. Energy Res.* **2019**, *43*, 2843−2853.

(34) Hellstern, T.; Gauthier, E.; Cheah, M. J.; Benziger, J. B. The role of the gas diffusion layer on slug formation in gas flow channels of fuel cells. *Int. J. Hydrogen Energy* **2013**, *38*, 15414−15427.

(35) Koido, T.; Furusawa, T.; Moriyama, K. An approach to modeling two-phase transport in the gas diffusion layer of a proton exchange membrane fuel cell. *J. Power Sources* **2008**, *175*, 127−136.

(36) Koido, T.; Furusawa, T.; Moriyama, K.; Takato, K. Two-phase transport properties and transport simulation of the gas diffusion layer of a PEFC. *ECS Trans.* **2006**, *3*, 425.

(37) Yu, H.; Ziegler, C.; Oszcipok, M.; Zobel, M.; Hebling, C. Hydrophilicity and hydrophobicity study of catalyst layers in proton exchange membrane fuel cells. *Electrochim. Acta* **2006**, *51*, 1199−1207.

(38) Medici, E. F.; Zenyuk, I. V.; Parkinson, D. Y.; Weber, A. Z.; Allen, J. S. Understanding Water Transport in Polymer Electrolyte Fuel Cells Using Coupled Continuum and Pore-Network Models. *Fuel Cells* **2016**, *16*, 725−733.

(39) Mortazavi, M.; Tajiri, K. Effect of the PTFE content in the gas diffusion layer on water transport in polymer electrolyte fuel cells (PEFCs). *J. Power Sources* **2014**, *245*, 236−244.

(40) Nagy, K. A.; Tóth, I. Y.; Ballai, G.; Varga, Á. T.; Szenti, I.; Sebők, D.; Kopniczky, J.; Hopp, B.; Kukovecz, Á. Wetting and evaporation on a carbon cloth type gas diffusion layer for passive direct alcohol fuel cells. *J. Mol. Liq.* **2020**, *304*, No. 112698.

(41) Gostick, J. T.; Ioannidis, M. A.; Fowler, M. W.; Pritzker, M. D. Wettability and capillary behavior of fibrous gas diffusion media for polymer electrolyte membrane fuel cells. *J. Power Sources* **2009**, *194*, 433−444.

(42) Gostick, J. T.; Ioannidis, M. A.; Fowler, M. W.; Pritzker, M. D. Direct measurement of the capillary pressure characteristics of water−air−gas diffusion layer systems for PEM fuel cells. *Electrochem. Commun.* **2008**, *10*, 1520−1523.

(43) Tranter, T.; Gostick, J.; Burns, A.; Gale, W. Capillary hysteresis in neutrally wettable fibrous media: a pore network study of a fuel cell electrode. *Transp. Porous Media* **2018**, *121*, 597−620.

(44) Battrell, L.; Zhu, N.; Zhang, L.; Anderson, R. Transient, spatially resolved desaturation of gas diffusion layers measured via synchrotron visualization. *Int. J. Hydrogen Energy* **2018**, *43*, 11234−11243.

(45) Manzi-Orezzoli, V.; Mularczyk, A.; Trtik, P.; Halter, J.; Eller, J.; Schmidt, T. J.; Boillat, P. Coating Distribution Analysis on Gas Diffusion Layers for Polymer Electrolyte Fuel Cells by Neutron and X-ray High-Resolution Tomography. *ACS Omega* **2019**, *4*, 17236−17243.

(46) Mularczyk, A.; Lin, Q.; Niblett, D.; Vasile, A.; Blunt, M. J.; Niasar, V.; Marone, F.; Schmidt, T. J.; Büchi, F. N.; Eller, J. Operando Liquid Pressure Determination in Polymer Electrolyte Fuel Cells. *ACS Appl. Mater. Interfaces* **2021**, *13*, 34003−34011.

(47) AlRatrout, A.; Raeini, A. Q.; Bijeljic, B.; Blunt, M. J. Automatic measurement of contact angle in pore-space images. *Adv. Water Resour.* **2017**, *109*, 158−169.

(48) Liu, C. P.; Saha, P.; Huang, Y.; Shimpalee, S.; Satjaritanun, P.; Zenyuk, I. V. Measurement of Contact Angles at Carbon Fiber−Water−Air Triple-Phase Boundaries Inside Gas Diffusion Layers Using X-ray Computed Tomography. *ACS Appl. Mater. Interfaces* **2021**, *13*, 20002−20013.

(49) Armstrong, R. T.; Porter, M. L.; Wildenschild, D. Linking pore-scale interfacial curvature to column-scale capillary pressure. *Adv. Water Resour.* **2012**, *46*, 55−62.

(50) Sun, C.; McClure, J. E.; Mostaghimi, P.; Herring, A. L.; Berg, S.; Armstrong, R. T. Probing effective wetting in subsurface systems. *Geophys. Res. Lett.* **2020**, *47*, No. e2019GL086151.

(51) Ali, K.; Bilal, S. Surface tensions and thermodynamic parameters of surface formation of aqueous salt solutions: III. Aqueous solution of KCl, KBr and KI. *Colloids Surf., A* **2009**, *337*, 194−199.

(52) (a) Park, J. W.; Jiao, K.; Li, X. Numerical investigations on liquid water removal from the porous gas diffusion layer by reactant flow. *Appl. Energy* **2010**, *87*, 2180−2186. (b) Tamayol, A.; McGregor, F.; Bahrami, M. Single phase through-plane permeability of carbon paper gas diffusion layers. *J. Power Sources* **2012**, *204*, 94−99.

(53) Mortazavi, M.; Tajiri, K. Liquid water breakthrough pressure through gas diffusion layer of proton exchange membrane fuel cell. *Int. J. Hydrogen Energy* **2014**, *39*, 9409−9419.

(54) Rofaiel, A.; Ellis, J.; Challa, P.; Bazylak, A. Heterogeneous through-plane distributions of polytetrafluoroethylene in polymer electrolyte membrane fuel cell gas diffusion layers. *J. Power Sources* **2012**, *201*, 219−225.

(55) De Arquer, F. P. G.; Dinh, C.-T.; Ozden, A.; Wicks, J.; McCallum, C.; Kirmani, A. R.; Nam, D.-H.; Gabardo, C.; Seifitokaldani, A.; Wang, X. CO2 electrolysis to multicarbon products at activities greater than 1 A cm− 2. *Science* **2020**, *367*, 661−666.

(56) Lim, A.; Jeong, H.-Y.; Lim, Y.; Kim, J. Y.; Park, H. Y.; Jang, J. H.; Sung, Y.-E.; Kim, J. M.; Park, H. S. Amphiphilic Ti porous transport layer for highly effective PEM unitized regenerative fuel cells. *Sci. Adv.* **2021**, *7*, No. eabf7866.

(57) Niblett, D.; Niasar, V.; Holmes, S. Enhancing the performance of fuel cell gas diffusion layers using ordered microstructural design. *J. Electrochem. Soc.* **2019**, *167*, No. 013520.

(58) Wildenschild, D.; Sheppard, A. P. X-ray imaging and analysis techniques for quantifying pore-scale structure and processes in subsurface porous medium systems. *Adv. Water Resour.* **2013**, *51*, 217−246.